nature physics

SUPPLEMENTARY INFORMATION

DOI: 10.1038/NPHYS1892

LOCALIZATION OF PREFORMED COOPER PAIRS IN DISORDERED SUPERCONDUCTORS

Benjamin Sacépé,[1,2,*] Thomas Dubouchet,[1] Claude Chapelier,[1] Marc Sanquer,[1] Maoz Ovadia,[2] Dan Shahar,[2] Mikhail Feigel'man,[3] and Lev Ioffe[4]

[1]*SPSMS, UMR-E 9001, CEA-INAC/ UJF-Grenoble 1, 17 rue des martyrs, 38054 GRENOBLE cedex 9, France*

[2]*Department of Condensed Matter Physics, The Weizmann Institute of Science, Rehovot 76100, Israel*

[3]*L. D. Landau Institute for Theoretical Physics, Kosygin str.2, Moscow 119334, Russia*

[4]*Serin Physics laboratory, Department of Physics and Astronomy, Rutgers University, Piscataway, NJ 08854, USA*

I. TRANSPORT MEASUREMENTS

In this section we present the transport properties of our highly disordered amorphous InO films. The temperature evolution of the resistivity for the three samples studied in this work are shown in Fig. S1. All films show the insulating trend: the resistivity increases as T is lowered from room temperature. Despite this clear signature of electron localization, the films undergo a superconducting transition with critical temperature $1-2\,K$ (see inset of Fig. S1). The continuous decrease of the critical temperature upon increasing disorder is the hallmark of the disorder-driven superconductor-insulator transition that occurs in our InO films.

II. SCANNING TUNNELING MICROSCOPY AND SPECTROSCOPY OF AMORPHOUS INDIUM-OXIDE FILMS

Scanning tunneling spectroscopy was performed in a home-built scanning tunneling microscope thermally anchored to the mixing chamber of an inverted dilution refrigerator. It is likely that a native layer of over-oxidized InO_x forms at the film surface when sample is exposed to air when transferred into the STM cryostat. Nevertheless one can achieve good tunneling conditions as shown by the topographic image in Fig. S2. The r.m.s. roughness of 7 Å demonstrates surface flatness.

At low temperature, the quality of the STM junction yields excellent tunneling spectroscopy as seen by the superconducting spectra shown in Fig. 1, Fig. S3, Fig. S4 and Fig. S5. The observation of a full gap is characteristic of a good tunneling barrier: it signals that superconductivity is not

DOI: 10.1038/NPHYS1892

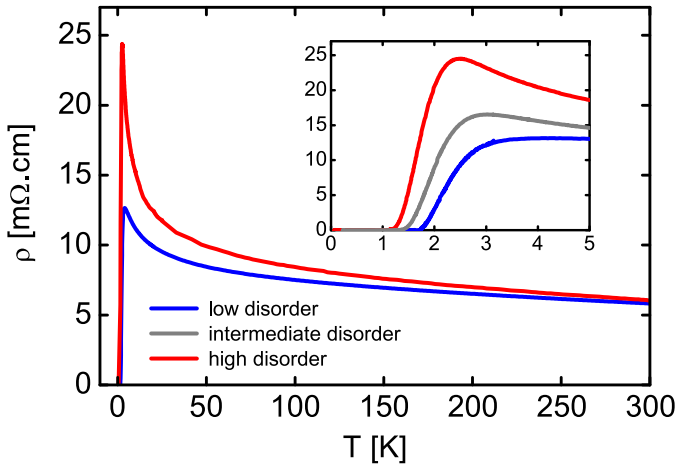

FIG. S1: **Resistivity versus temperature of amorphous indium oxyde films.** Thicknesses of the samples are 150 Å for low disorder sample and 300 Å for high and intermediate disorder samples. Inset: superconducting transitions measured during the cooling of the STM setup. The critical temperatures defined as the vanishing resistance (see main text) are $1.7\,K$, $1.4\,K$ and $1.2\,K$ for low, intermediate and high disorder sample respectively.

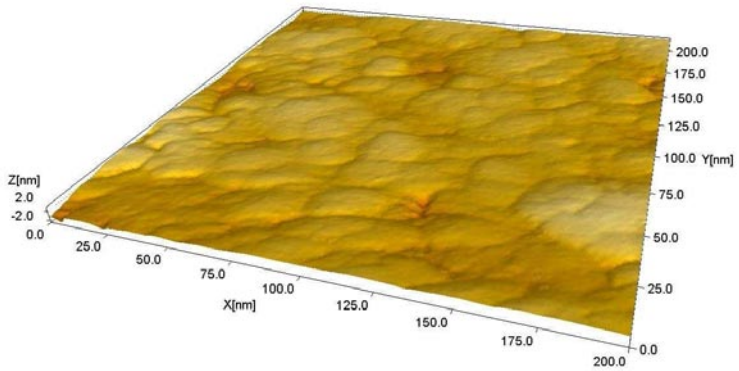

FIG. S2: **Surface topography.** Topographic image ($200 \times 200\,nm^2$) of sample low disorder obtained at room temperature. The r.m.s. roughness of the surface is 7Å.

weakened at the surface of the InO films due to air exposure. A damaged metallic surface coupled to the film with a proximity-induced superconducting DoS would have led to a reduced Δ/T_c ratio as well as a non-zero DoS at the Fermi level. The large Δ/T_c ratio (shown in Fig. 4a) and the lack of states at the Fermi level in our measurements imply very good tunneling conditions. In addition we note that the diffusive length in the millivolt range is of the order of few nanometers ensuring that tunneling electrons probe the physical properties of the film (to estimate the diffusion length we use the density of states[1] $\nu \sim 10^{21}\,(eV)^{-1}cm^{-3}$ that gives the diffusion coefficient $D \sim 1\,cm^2s^{-1}$

and thus the diffusion length $l \sim 8\,nm$ at $1\,meV$).

III. SPATIAL FLUCTUATIONS OF THE LOCAL DENSITY OF STATES

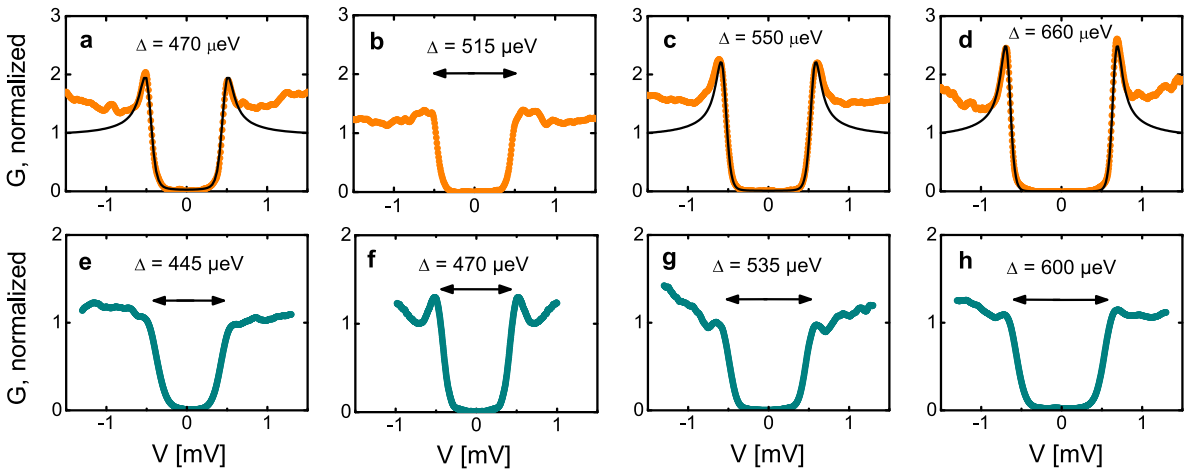

FIG. S3: **Fluctuations of gap and coherence peak height.** Individual raw tunneling spectra measured at different locations on low disorder (**a-d**) and on high disorder (**e-h**) samples. In the locations where coherence peaks are pronounced, a fit with the theoretical *s*-wave BCS DoS (ref. [2]) can be used to evaluate the gap amplitude. Beyond the gap, the tunneling conductance increases slowly upon an increase in the bias voltage V leading to a discrepancy with the BCS fit. This increasing spectral weight has also been observed in TiN films[3] and in quench condensed Bi films[4]. It might be due to a contribution of the disorder-enhanced Coulomb interaction which yields a depression of the DoS that is maximum at zero bias and extends up to energies much higher than the energy scale probe in this study, the effect known as zero-bias anomaly[5].

In this section we focus on the spatial evolution of the spectral properties. All spectroscopy data presented in this work were obtained by measuring the differential conductance of the tunneling junction in a scan area of $3 \times 3\,\mu m^2$. For instance, the statistical analysis presented in Fig. 2 results from a collection of individual spectra acquired systematically at different locations in such area. To illustrate the different spectra that contribute to the statistical analysis, we show in figure S3 a set of typical spectra measured at $50\,mK$ for samples of low and high disorder that exhibits strong variations in the gap amplitude and coherence peaks height. For instance the spectra a and d, with gap values of $470\,\mu eV$ and $660\,\mu eV$ respectively, represent one of the smallest and one of the largest gaps observed in the low disorder sample (Fig. 2a). We observe that despite such a remarkably large variation, no change in the overall shape of the gap occurs except the coherence

DOI: 10.1038/NPHYS1892

peaks height. Fig. S3e-h show typical spectra observed in the high disorder sample where the local density of states is dominated by gaps with small peaks or with no peaks at all.

Our statistical analysis shows that the areas characterized by incoherent spectra take over the superconducting ones upon approaching the SIT. To give a feeling on the spatial structure of these areas, we show in Fig. S4 two traces of spectra acquired over 400 and 300 nm lines on the low disorder sample. Both gap and coherence peaks height fluctuations are clearly visible. One observes the intervals of the order of $50-100nm$ where coherent peaks are absent while the gap at the Fermi level remains. We believe that in these areas the electrons are bound in Cooper-pairs but are not coherently coupled to the surrounding superconducting condensate.

The length scale over which coherence peaks decrease is the relevant microscopic length scale for the loss of the superconducting coherence. We estimate from figure S4 that this length is of the order of $20-50\,nm$. On the other hand, there is no typical length scale associated to the gap fluctuations since they occur both at low scale ($\sim 20\,nm$) and at medium scale ($\sim 100\,nm$) as seen by the black lines of the contour plots in Fig. S4, and as expected if the measurement probes the electrons characterized by the wave function of fractal nature.

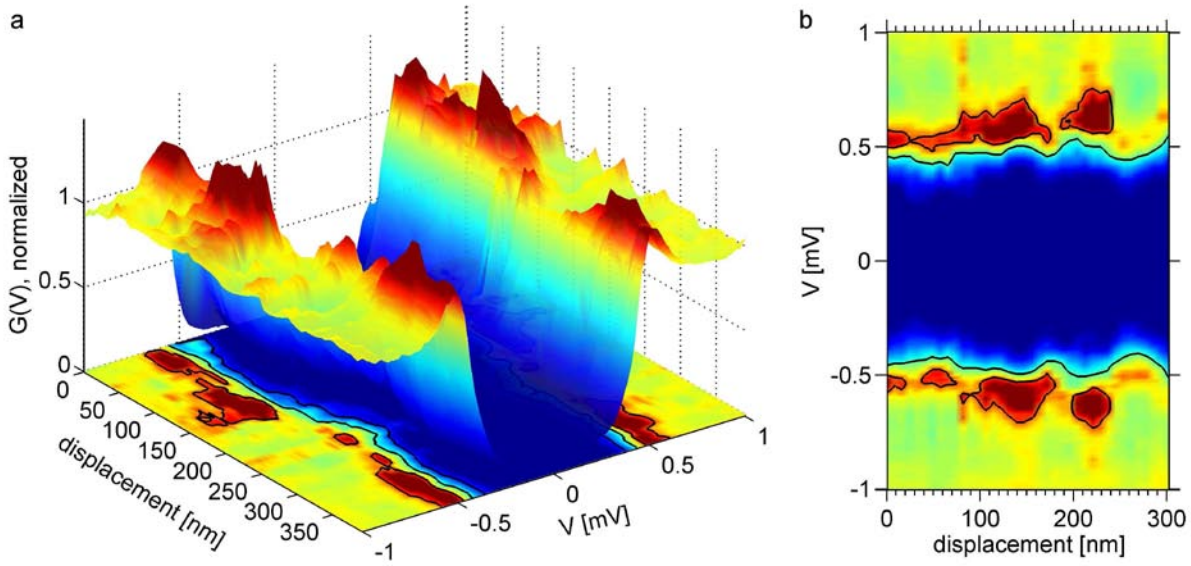

FIG. S4: **Visualization of localized Cooper-pairs area. a**, Three-dimensional plot of 50 spectra acquired at $50\,mK$ over a line of $400\,nm$. The tunneling conductance is plotted versus bias voltage and the tip displacement. **b**, Two-dimensional view of the tunneling conductance for a different line of $300\,nm$ long. The colorscale corresponds to the one in **a**. In both figures, black lines correspond to iso-differential conductance curves that emphasize the gap and coherence peaks height fluctuations.

IV. APPEARANCE OF COHERENCE PEAK AT T_{peak}

Data presented in Figure 4 come from a set of temperature evolutions of the DoS measured at separate locations on the samples. The measurements were performed by controlling the temperature of the sample with a resistive heater and a RuO_2 thermometer that are glued onto the STM sample holder. Starting from the base temperature with the STM tip at a fixed location, the samples were warmed up in small steps at which the differential conductance of the tunneling junction was measured. The small thermal coupling between the STM sample holder and the mixing chamber of the dilution refrigerator allowed us to reach the temperatures up to $6\,K$ for a short period of time. The total acquisition time of a T-evolution from $50\,mK$ up to $6K$ was about 2 hours for about a hundred spectra, followed by the time required to recover the base T. Unfortunately, our dilution refrigerator setup precludes measurements at fixed temperatures above $1\,K$ during long periods of time due to instabilities of the fridge that occur when the heat load is held on for a long period of time.

In figure S5 we show an additional set of temperature evolutions of the DoS that were used to determine the temperature T_{peak} below which coherence peaks start to grow (plotted in Fig. 4a). The figures (a-d) and (e-f) show the data for the high disorder and low disorder samples respectively. Notice that for low disorder sample two locations corresponding to Fig. 1a and in Fig. S5e were measured are $600\,nm$ far apart, thus excluding any correlations that could explain the coincidence of their T_{peak}. The spectra measured at T_c are highlighted by the black dashed lines in Fig. S5. They clearly coincide with the beginning of the coherence peaks growth at T_{peak} independently of the gap value, the coherence peaks height or the STM tip location.

V. SUMMARY OF THE THEORY OF SUPERCONDUCTIVITY CLOSE TO THE MOBILITY EDGE

Here we sketch the main ingredient of the theory developed in Ref. 6-9 and its application to the data. In the range of a strongly developed pseudogap $\Delta_P \gg T_c$ electron "orbitals" $\psi_j(\mathbf{r})$ are populated by either zero or two electrons at low T's. In this case the whole Hilbert space of the electronic problem reduces to the "pseudospin" subspace described by operators formally equivalent to spin-$\frac{1}{2}$ variables $S_j^{\pm}, S_j^z$ associated with each orbital: $S_j^+ = c_{\uparrow,j}^+ c_{\downarrow,j}^+$ is the pair creation operator and $2S_j^z = c_{\uparrow,j}^+ c_{\uparrow,j} + c_{\downarrow,j}^+ c_{\downarrow,j} - 1$; this representation was proposed originally by Anderson[10].

DOI: 10.1038/NPHYS1892

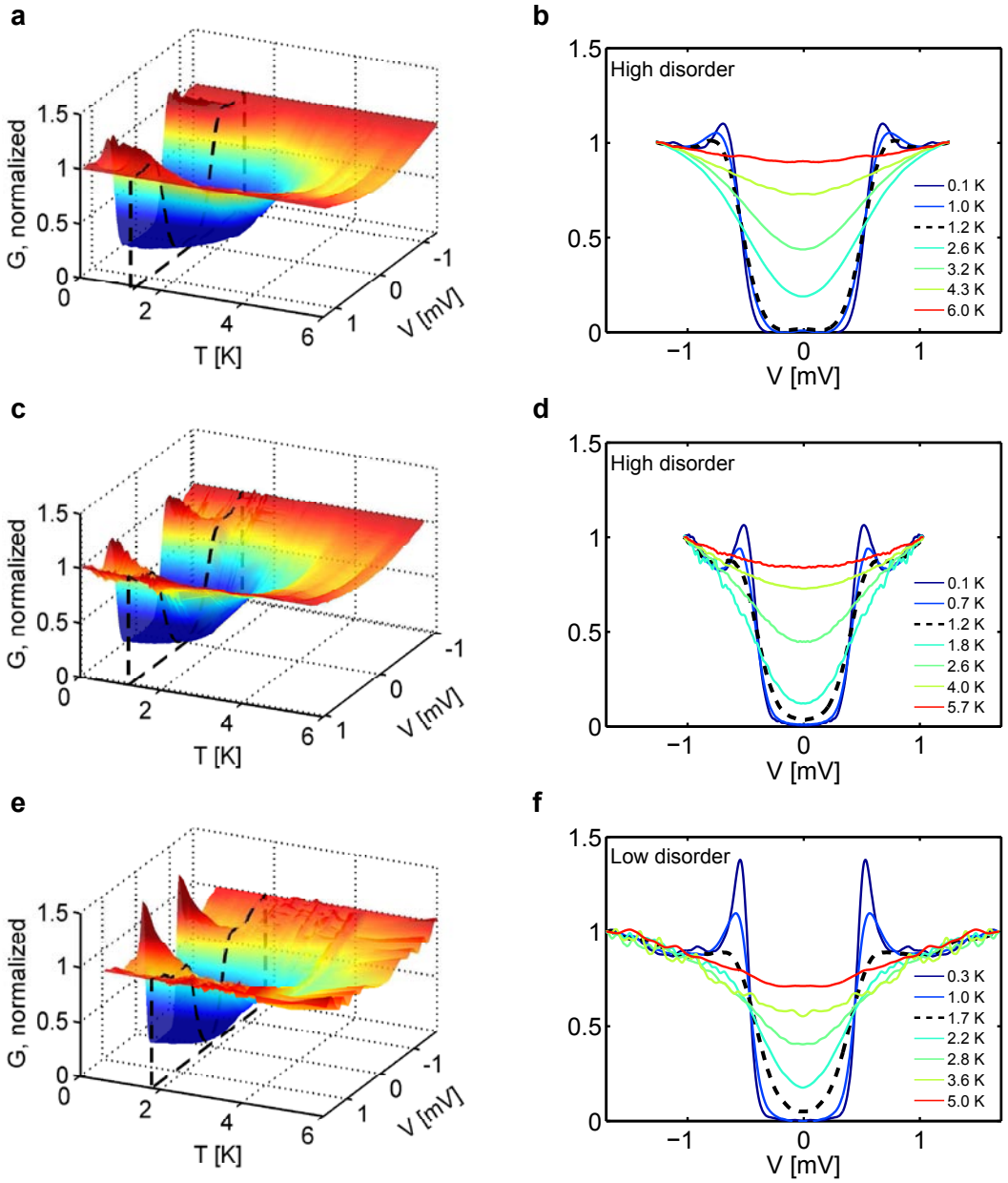

FIG. S5: T**-evolution of the tunneling spectra.** Temperature evolution of the normalized tunneling conductance G measured in sample high disorder (**a-d**), and in sample low disorder (**e**,**f**). Each set shows the spectra are measured at a single location on the sample surface without any averaging. The black dashed lines show the spectra measured at T_c. The gap values Δ, the ratios $2\Delta/T_c$ and T_{peak}/T_c are respectively: (**a**,**b**) 600 μeV, 11.3, 1.09, (**c**,**d**) 450 μeV, 8.6, 1.02, and (**e**,**f**) 500 μeV, 6.6, 0.99.

The development of superconducting coherence is described by the pseudospin Hamiltonian

$$H_{PS} = 2\sum_j \epsilon_j S_j^z - \frac{g}{2}\sum_{ij} M_{ij}(S_i^+ S_j^- + S_i^- S_j^+), \qquad (1)$$

with matrix elements $M_{ij} = \int d^3\mathbf{r}\psi_i^2(\mathbf{r})\psi_j^2(\mathbf{r})$ and coupling constant g. On-site energies ϵ_j are distributed over wide band with bare DoS ν_0. The pseudogaped regime $\Delta_P \gg T_c$ is realized[6,7] when typical level spacing inside localization volume, $\delta \sim 1/\nu_0\xi_{loc}^3$, is the largest energy scale, $\delta \gg \Delta_P$. The local pairing fields $h_j(T)$ determine the average transverse pseudospin component via $\langle S_i^x\rangle = (h_i/2E_i)\tanh(E_i/T)$; they obey self-consistency equation

$$h_i = \frac{g}{2}\sum_j M_{ij}\frac{h_j}{E_j}\tanh\frac{E_j}{T}\,, \quad E_j = \sqrt{h_j^2+\epsilon_j^2}. \tag{2}$$

At very large δ, long-range coherence is not established even at $T = 0$, and insulating ground state takes over. The quantum phase transition between the ordered state with non-zero $\langle S^{x,y}\rangle \neq 0$ and disordered one with $\langle S^{x,y}\rangle = 0$ was studied in Ref.[8,9] within the simplified model defined by the Hamiltonian (1) on the Bethe lattice with coordination number K and all nonzero couplings $M_{ij} = 1/K$. The model is characterized by dimensionless coupling $\lambda = g\nu_0 \ll 1$. The result of this study is that in the limit $K > K_1 = \lambda e^{1/2\lambda}$ usual BCS-like mean-field theory works well and uniform superconducting state occurs below $T_{c0} = \nu_0^{-1}e^{-1/\lambda}$. In particular, below T_{c0} nonzero thermal average $h_j(T)$ appear.

Fluctuations become important at $K < K_1 = \lambda e^{1/2\lambda}$. They lead to two effects: the critical temperature $T_c(K)$ start to drop down with K decrease and the order parameter $h_i(T)$ becomes strongly inhomogeneous as a function of the site number i and cannot be expressed in terms of local energy ϵ_j only. Eventually, the transition temperature vanishes at $K = K_2 = \lambda e^{1/e\lambda}$, the ground-state at $K < K_2$ is a many-body insulator, with discrete spectrum of low-lying excitations.

In the whole region $K_2 < K < K_1$ on the superconducting side of quantum phase transition, a nonzero order parameter $h_j(T)$ appears below the well-defined global transition temperature $T_c(K)$ and leads to the growth of coherence peaks seen in the tunneling spectra, Fig. 1a,c. At the same time, the relative heights of these peaks are proportional to the values of $h_j(T)$ for the electron orbitals $\psi_j(\mathbf{r})$ which have considerable weights near the tip position $\mathbf{r}$. The values of h_j fluctuate strongly between different sites j with very close local energies ϵ_j. The strength of these fluctuations is characterized by the distribution function $P(h)$ with a long tail: close to the transition line $T_c(K)$ the distribution is $P(h) \sim (1/h_0)(h_0/h)^\alpha$ in a wide range of h/h_0. The exponent α decreases with the decrease of K, i.e. in physical terms, with the increase of disorder. In particular, at $K_2 < K < K_1$ the exponent $1 < \alpha < 2$ was found[8,9], indicating that a simple average $h_{av} = \langle h\rangle$ and typical value $h_{typ} = exp(\langle\log(h)\rangle)$ differ qualitatively, with $h_{typ} \ll h_{av}$ (h_{typ} characterizes behaviour of *almost any* specific sample, whereas h_{av} corresponds to a contribution of extremely rare fluctuations in the ensemble average over many samples). We show in Fig. 3

DOI: 10.1038/NPHYS1892

theoretical results for two nearby values of the coordination number $K = 5$ and $K = 6$, both at the dimensionless coupling constant $\lambda = 0.128$. While the values of the critical temperature are close in these two cases ($T_c(K = 5)/T_c(K = 6) \approx 0.9$), the shape of $P(h)$ distribution changes considerably: the "tail" with $h \ll h_{typ}$ becomes much more pronounced for the $K = 5$ case that corresponds to stronger disoder. This theoretical result is in good agreement with our observations shown in Fig. 2b,d: distribution of peak heights is moderately narrow in the less disordered sample shown in Fig. 2b and becomes very broad (like the $P(h)$ distribution function at $K < K_1$) for the more disordered sample in Fig. 2d.

---

* Present address: Institut Néel, CNRS and Université Joseph Fourier, BP 166, 38042 Grenoble, France

[1] Ovadyahu, Z. Private communication.

[2] Bardeen, J., Cooper, L. N., Schrieffer, J. R. Theory of Superconductivity. *Phys. Rev.* **108,** 1175–1204 (1957).

[3] Sacépé, B. *et al.* Disorder-Induced Inhomogeneities of the Superconducting State Close to the Superconductor-Insulator Transition. *Phys. Rev. Lett.* **101,** 157006 (2008).

[4] Valles, J. M., Dynes, R. C., Garno, J. P. Electron tunneling determination of the order-parameter amplitude at the superconductor-insulator transition in 2D. *Phys. Rev. Lett.* **69,** 3567–3570 (1992).

[5] Altshuler, B., Aronov, A. G., Lee, P. A. Interaction effects in disordered Fermi systems in two dimensions. *Phys. Rev. Lett.* **44,** 1288–1291 (1980).

[6] Feigel'man, M. V., Ioffe, L. B., Kravtsov, V. E., Yuzbashyan, E. A. Eigenfunction Fractality and Pseudogap State near the Superconductor-Insulator Transition. *Phys. Rev. Lett.* **98,** 027001 (2007).

[7] Feigel'man, M. V., Ioffe, L. B., Kravtsov, V. E., Cuevas, E. Fractal superconductivity near localization threshold. *Annals of Physics* **325,** 1390–1478 (2010).

[8] Ioffe, L. B., Mézard, M. Disorder-Driven Quantum Phase Transitions in Superconductors and Magnets. *Phys.Rev. Lett.* **105,** 037001 (2010).

[9] Feigel'man, M. V., Ioffe, L. B., Mezard, M. Superconductor-insulator transition and energy localization, arXiv:1006.5767.

[10] Anderson, P. W. Random-Phase Approximation in the Theory of Superconductivity. *Phys. Rev.* **112.** 1900–1916 (1958).